Vol. 611: 31–44, 2019
https://doi.org/10.3354/meps12868

MARINE ECOLOGY PROGRESS SERIES
Mar Ecol Prog Ser

Published February 14

Effects of microbial processes and $CaCO_3$ dynamics on inorganic carbon cycling in snow-covered Arctic winter sea ice

Dorte Haubjerg Søgaard[1,2,*], Jody W. Deming[3], Lorenz Meire[1,4], Søren Rysgaard[1,2,5]

[1]Greenland Climate Research Centre (C/O Greenland Institute of Natural Resources), Kivioq 2, PO Box 570, 3900 Nuuk, Greenland

[2]Arctic Research Centre, Department of Bioscience, Aarhus University, Ny Munkegade 116, building 1540, 8000 Aarhus C, Denmark

[3]School of Oceanography, University of Washington, Seattle, WA 98195, USA

[4]Royal Netherlands Institute for Sea Research, and Utrecht University, 4401 NT Yerseke, Netherlands

[5]Centre for Earth Observation Science, CHR Faculty of Environment Earth and Resources, University of Manitoba, 499 Wallace Building, Winnipeg, MB R3T 2N2, Canada

ABSTRACT: Few combined measurements of primary and bacterial productivity exist for Arctic sea ice, particularly during winter, making it difficult to assess the relative importance of these microbial processes for carbon cycling in sea ice. Furthermore, the occurrence of calcium carbonate ($CaCO_3$), though well-documented in sea ice, is poorly described for the overlying snow. To address these gaps, we investigated primary and bacterial productivity and carbon dynamics at 2 contrasting locations: (1) a landfast site, with thick snow-covered first-year sea ice, and (2) a polynya site, with thin snow-covered young (<1 wk) sea ice. Comparisons of bacterial carbon demand and primary production indicated net heterotrophy in the sea ice at both locations, with a net carbon consumption rate of 0.87 to 1.86 mg C m^{-2} d^{-1} derived from sea ice bacterial carbon demand of 0.93 to 2.00 mg C m^{-2} d^{-1} and gross primary production of 0.06 to 0.14 mg C m^{-2} d^{-1}. As these microbial rates are very low, physical processes largely account for the observed CO_2 depletion in the ice. High $CaCO_3$ concentrations of 250 to 430 µmol kg^{-1} were measured in the snow covers which, though similar to concentrations in the underlying ice, are orders of magnitude higher than those reported from the few studies available on $CaCO_3$ in snow. Together these results suggest that the role of biology in modulating inorganic carbon cycling in ice, which can be important in spring, is minor as compared to abiotic processes.

KEY WORDS: High Arctic · First-year sea ice · Polynya ice · Snow cover · Primary production · Bacterial production · $CaCO_3$

1. INTRODUCTION

Recent studies have demonstrated that seasonal sea ice dynamics may significantly affect the air–sea exchange of CO_2 (e.g. Sievers et al. 2015, Grimm et al. 2016). Brine pCO_2 within the ice can be influenced strongly by abiotic processes, such as brine drainage and $CaCO_3$ precipitation and dissolution, but also by biotic processes, especially in areas and seasons with high biological activity (Miller et al. 2011, Papadimitriou et al. 2012, Søgaard et al. 2013). During winter, low temperatures decrease the brine volume and concurrently increase the salinity and gas content of the brine (e.g. Weeks & Ackley 1986, Petrich & Eicken 2010). As sea ice grows, brine drainage leads to an export of gases from the sea ice,

*Corresponding author: doso@natur.gl

Publisher: Inter-Research · www.int-res.com

leaving sea ice depleted in CO_2 compared to ambient seawater (Rysgaard et al. 2007). During spring, undersaturated sea ice meltwater therefore represents a sink for CO_2, gradually re-equilibrating with the atmosphere and underlying water over time (e.g. Geilfus et al. 2016, Grimm et al. 2016).

$CaCO_3$ precipitation in brines, however, can further complicate this conceptual understanding of sea ice-associated CO_2 dynamics. As temperature decreases and solute concentration increases, $CaCO_3$ precipitates (Marion 2001). During $CaCO_3$ formation, CO_2 is released to the aqueous phase, which raises pCO_2 and decreases the total alkalinity (TA) to total carbon dioxide (TCO_2) ratios within the brine. Respiration may also raise pCO_2 (Miller et al. 2011). However, CO_2 is rejected more efficiently from the ice than TA, because alkalinity is trapped in $CaCO_3$ crystals within the interstices between the ice crystals (Rysgaard et al. 2013) leading to high TA:TCO_2 ratios in sea ice and high pCO_2 levels in the underlying water (Rysgaard et al. 2009). Brine drainage from sea ice causes the formation of highly saline dense cold water that together with CO_2 sinks below the pycnocline and, subsequently, may be incorporated into intermediate and deep water masses (Rysgaard et al. 2007).

During spring, when sea ice begins to melt, the dissolution of $CaCO_3$ (e.g. Geilfus et al. 2016), autotrophic assimilation of CO_2 (e.g. Gradinger 2009, Campbell et al. 2016), and dilution of brine by undersaturated meltwater are all processes that can decrease the pCO_2 of the brines and, ultimately, of the surface waters (Nomura et al. 2010b). A lowering of the surface seawater CO_2 in turn leads to an increase in the air–sea flux of CO_2 (e.g. Grimm et al. 2016).

Sea ice is a low-temperature habitat characterized by steep physical and chemical gradients hosting diverse microbial communities of bacteria, archaea, and eukaryotic microalgae (Collins et al. 2010, Eronen-Rasimus et al. 2014). Both bacterial production and algal production influence the overall productivity of the marine system. Bacteria typically contribute less than 10% of the total productivity in sea ice during spring and summer, but they can account for most of the total productivity during winter—based on the few studies available for that season (Deming 2010). Sea ice algae account for most of the production in the ice during spring and contribute up to 60% of the total integrated primary production (pelagic and sea ice) of high Arctic ecosystems (Fernandez-Mendez et al. 2015). In coastal Greenlandic waters, the ice-algal contribution appears to be much less, amounting for 1 to 24% of the total integrated production (Mikkelsen et al. 2008, Arrigo 2017).

During mid-winter the sea ice cover in central Young Sound, NE Greenland, is between 100 and 160 cm thick and covered by 20 to 100 cm of snow. In recent decades Young Sound has experienced increasing air temperatures, with temperatures ~1.2°C above the 1996 to 2002 average, especially during summer and autumn (Jensen et al. 2013). This increase has resulted in an overall reduction in ice thickness and longer ice-free periods in this area.

The area outside Young Sound is a polynya site, where new sea ice is produced and frequently blown away, thereby allowing new ice to form repeatedly (Dmitrenko et al. 2015). Five polynya sites are reported from East Greenland (Sørensen 2012); however, knowledge of the biotic and abiotic processes in the sea ice in these areas is lacking.

The objective of this study was to quantify the algal and bacterial productivity in late winter in thick first-year sea ice (FYI) and in thin, newly formed sea ice in a polynya to investigate the potential influence of these microbial processes on carbon turnover. We also aimed to understand the role of $CaCO_3$ not only in the sea ice but also in the snow cover overlying these 2 types of winter sea ice formations.

2. MATERIALS AND METHODS

2.1. Study site and sampling

Sampling was conducted at 2 contrasting locations in Young Sound (74° N, 20° W), NE Greenland, as described in detail by Rysgaard et al. (2013), during an ice campaign in March 2012. The first site, characterized by landfast FYI, was called ICE I (74° 18.57′ N, 20° 18.27′ W; see Fig. S1 in the Supplement at www.int-res.com/articles/suppl/m611p031_supp.pdf). The second site, located in a polynya area about 3 km from the landfast ice edge, was called POLY I (74° 13.905′ N, 20° 07.701′ W; Fig. S1). In this polynya area, the sea ice breaks up regularly during winter (for more details see Pedersen et al. 2010, Rysgaard et al. 2013). Oceanographic conditions below sea ice at this site during winter and spring have been reported by Dmitrenko et al. (2015) and Boone et al. (2017).

Sea ice cores were collected at each station on 3 days (18, 20 and 24 March 2012) using a MARK II coring system (Kovacs Enterprises) within a defined area (5 m^2). On each day triplicate cores were collected for physical and chemical samples. Duplicate

cores were collected for biological parameters. The overlying snow cover was collected at both stations using a small alkali-washed shovel. The under-ice seawater samples were collected using a Niskin (General Oceanics) water sampler at 2 depths: 5 m and 20 m.

2.2. Abiotic parameters

The air temperature was measured 2 m above the snow, and vertical profiles of temperature within the ice were measured using a thermometer (Testo). Light attenuation of the snow cover was determined by measuring downwelling irradiance directly above and below the snow with a data logger (LI–1400, Li-Cor Biosciences). One of the sea ice cores was cut into 12 cm sections using a stainless steel saw and placed in a specially designed container which only allowed light to enter from above. Light attenuation was measured with a Li-Cor quantum 2 pi sensor connected to a LI–1400 data logger (Li-Cor Biosciences) directly above and below the ice section. The sea ice sections were placed in plastic containers and transported back to the laboratory in thermally insulated boxes. To determine TA and TCO_2 concentrations in sea ice, 3 sea ice cores were cut into 5 to 10 cm sections, placed immediately in gas-tight plastic bags (Rysgaard et al. 2013), and transported back to the laboratory in thermally insulated boxes. In the laboratory, sea ice sections were weighed for later determination of density and then melted in the dark at 3 ± 1°C over a 2 d period. Conductivity of melted sea ice was measured (Thermo Orion Star with an Orion 013610MD conductivity cell) and converted to bulk salinity (Grasshoff et al. 1983).

Profiles based on triplicate samples of TCO_2 and TA in the sea ice are reproduced from Rysgaard et al. (2013). The deficit in TCO_2 concentration relative to surface TCO_2 concentration was calculated using bulk sea ice and water-column conditions of TCO_2 and salinity conditions at ICE I and POLY I. We used the water-column conditions at both sites as initial conditions from which sea ice was formed upon freezing (Rysgaard et al. 2011).

For both sampling stations, overlying snow cover was melted in the dark at 3 ± 1°C over a 2 d period to determine $CaCO_3$ concentration. The melted snow (200–500 ml) was filtered (at 3 ± 1°C) through precombusted (450°C, 6 h) Whatman GF/F filters. The exact volume of the filtered snow meltwater was measured. The filters were transferred to glass vials (12 ml Exetainer) containing 12 ml deionized water with a known TCO_2 concentration and 20 µl $HgCl_2$ (5% w/v, saturated solution) to avoid microbial activity during storage. The tubes were then spiked with 300 µl of 8.5% phosphoric acid and immediately closed to convert $CaCO_3$ on the filters to CO_2. After coulometric analysis of CO_2, the $CaCO_3$ concentration in snow cover was calculated as TCO_2 in the vial minus TCO_2 initially present in the deionized water (Johnson et al. 1993). A snow density of 0.30 g cm^{-3} (Kern et al. 2015) was used to convert $CaCO_3$ concentration in the melted samples to units of µmol kg^{-1}, to enable comparison to $CaCO_3$ concentrations in the underlying sea ice using comparable units (Rysgaard et al. 2013). Average values of triplicate samples are reported. The samples were inspected under a microscope (Leica DMiL LED) at 100 to 400 magnification as they were also allowed to melt. If crystals were dissolving, they were assumed to be $CaCO_3$. The samples were also checked for the presence of microorganisms with external structures of calcium carbonate, such as coccolithophores and foraminifers; none were detected in any of the snow samples.

2.3. Chemical and biotic parameters

Sections from 3 sea ice cores were melted in the dark at 3 ± 1°C over a 2 d period for measurements of dissolved organic carbon (DOC), dissolved organic nitrogen (DON) and the inorganic nutrients phosphate (PO_4^{3-}), silicic acid ($Si(OH)_4$) and nitrate and nitrite (NO_x). Sections from 2 sea ice cores were similarly melted for measurements of both primary and bacterial production and for chl *a* concentration and bacterial abundance.

DOC and DON were determined as in Søgaard et al. (2013). Average values of triplicate samples are reported. For determination of inorganic nutrients, triplicate samples of 10 ml were filtered onto 25 mm Whatman GF/F filters. The filtered samples were frozen (–19°C) for later analysis, using standard methods described in Søgaard et al. (2013). Average values of triplicate samples are reported.

Primary production was determined in melted sea ice samples at 3 light intensities (42, 21, 9 µmol photons m^{-2} s^{-1}) and corrected to dark incubation using the $H^{14}CO_3$ incubation technique (Steemann Nielsen 1952), and following the primary production procedure described by Søgaard et al. (2010). The potential primary production (in µg C l^{-1} h^{-1}) measured in the laboratory for different sea ice depths was plotted against the 3 laboratory light intensities and fitted to the function described by Platt et al. (1980). An esti-

mate of *in situ* primary production was calculated for each hour and sea ice depth using hourly *in situ* PAR irradiance. Average values of duplicate samples are reported.

Chl *a* concentration in each melted sea ice section and the under-ice seawater samples was determined on 2 occasions at both ICE I and POLY I. A volume of 50 ml of the melted sea ice for each of the sea ice sections, or 1000 ml for seawater, was filtered onto 25 mm Whatman GF/F filters for chl *a* analysis, as described by Søgaard et al. (2013). Average values of duplicate samples are reported. The measured rates of primary production were scaled to algal biomass to compare cell-specific rates between the ICE I and POLY I locations.

Bacterial production was calculated from a 6 h dark incubation period of melted sea ice samples (10 ml) with 10 nM of labeled [^{3}H] thymidine (New England Nuclear, specific activity 10.1 Ci mmol^{-1}), following the bacterial production procedure described by Søgaard et al. (2010). Triplicate blanks were fixed with trichloroacetic acid (1 ml of 50% TCA) prior to incubation, and duplicate sea ice samples were fixed with TCA immediately afterward. The samples were filtered through 0.2 µm cellulose ester filters that were rinsed with TCA prior to 22 h extraction in scintillation liquid (Ultima Gold, PerkinElmer) and measurement of activity on a liquid scintillation analyzer (TricCarb 2800, PerkinElmer). Bacterial carbon production was calculated using equations provided in Søgaard et al. (2010), with a conversion factor of 2.09×10^{18} cells mol^{-1} ^{3}H and carbon conversion factor of 5.7×10^{-8} µg C cell^{-1} as presented in Smith & Clement (1990). Bacterial carbon demand (in µg C kg^{-1} d^{-1}) was calculated using the equation provided in Nguyen & Maranger (2011) and a bacterial growth efficiency (BGE) of 0.5, as measured in polar oceans according to Rivkin & Legendre (2001). Average values of duplicate samples are reported.

For bacterial abundance measurements, samples of melted sea ice and snow and of underlying seawater were fixed with formaldehyde (final concentration of 2%) and stored dark and cold (3 ± 1°C). For snow samples, bulk salinity was determined by refractometer, as in Ewert et al. (2013), prior to fixation. Fixed samples were stained for DNA using the dual-staining approach described by Collins et al. (2008) for sea ice and seawater and by Ewert et al. (2013) for sea ice and snow. Bacteria were counted using DAPI optics, discriminating cells from other particles visualized only by AO optics. Samples were analyzed within 2 months of collection. Average values of duplicate samples are reported. The estimates of bacterial carbon demand were scaled to bacterial abundance to compare cell-specific rates between the ICE I and POLY I locations.

Pearson's correlation was used to identify significant ($p < 0.05$) relationships between each of the parameters measured in sea ice. Separate analyses were run for data from ICE I and from POLY I.

In summary, triplicate cores were collected on 18, 20 and 24 March 2012 to determine snow and ice thickness, ice temperature and bulk ice salinity. Additional triplicate cores were sampled to determine TCO_2 and TA concentrations, while 3 more cores were sampled for DOC, DON and inorganic nutrients. Further separate duplicate cores were sampled for measurements of primary production, bacterial production, chl *a* concentration and bacterial abundance.

3. RESULTS

3.1. Abiotic parameters at two contrasting sites

Snow temperature increased from −18°C at the top of the snowpack to −5°C at the snow–ice interface (Fig. 1a). Sea ice temperature at ICE I increased from −10°C at the top to −2°C at the ice–water interface (Fig. 1a); ice temperature at POLY I was generally higher, and increased from −5 to −2°C (Fig. 1a). Bulk salinity in snow was below detection at the top of the snowpack at both sites and increased to 32 at ICE I and 35.5 at POLY I at the snow–ice interface (see Table S1 in the Supplement). Bulk salinity in sea ice at ICE I ranged from 4 in surface ice to 9 in bottom ice (Fig. 1b). At POLY I, bulk salinity was higher, ranging from 7 in the surface to 10 in the bottom (Fig. 1b).

The snow cover caused strong light attenuation at both ICE I and POLY I, with attenuation coefficients ranging from 19 m^{-1} to 34 m^{-1} (Fig. 1c). In the sea ice, attenuation coefficients were higher at POLY I, with an average value of 13 m^{-1}, compared to the ICE I ice with an average attenuation coefficient of 4 m^{-1} (Fig. 1c).

3.2. Chemical parameters

All values in this section are reported as mean ± SD for melted sea ice (or snow) samples. At both sites, the TCO_2 and TA were highest in the bottom of the sea ice: 535 ± 2.4 and 628 ± 0.6 µmol kg^{-1} at ICE I and 570 ± 3.1 and 690 ± 7.3 µmol kg^{-1} at POLY I, respectively (Fig. 2). These values decreased to 256 ± 5.1 and 380 ± 2.4 µmol kg^{-1} at ICE I, and to 440 ± 5.3

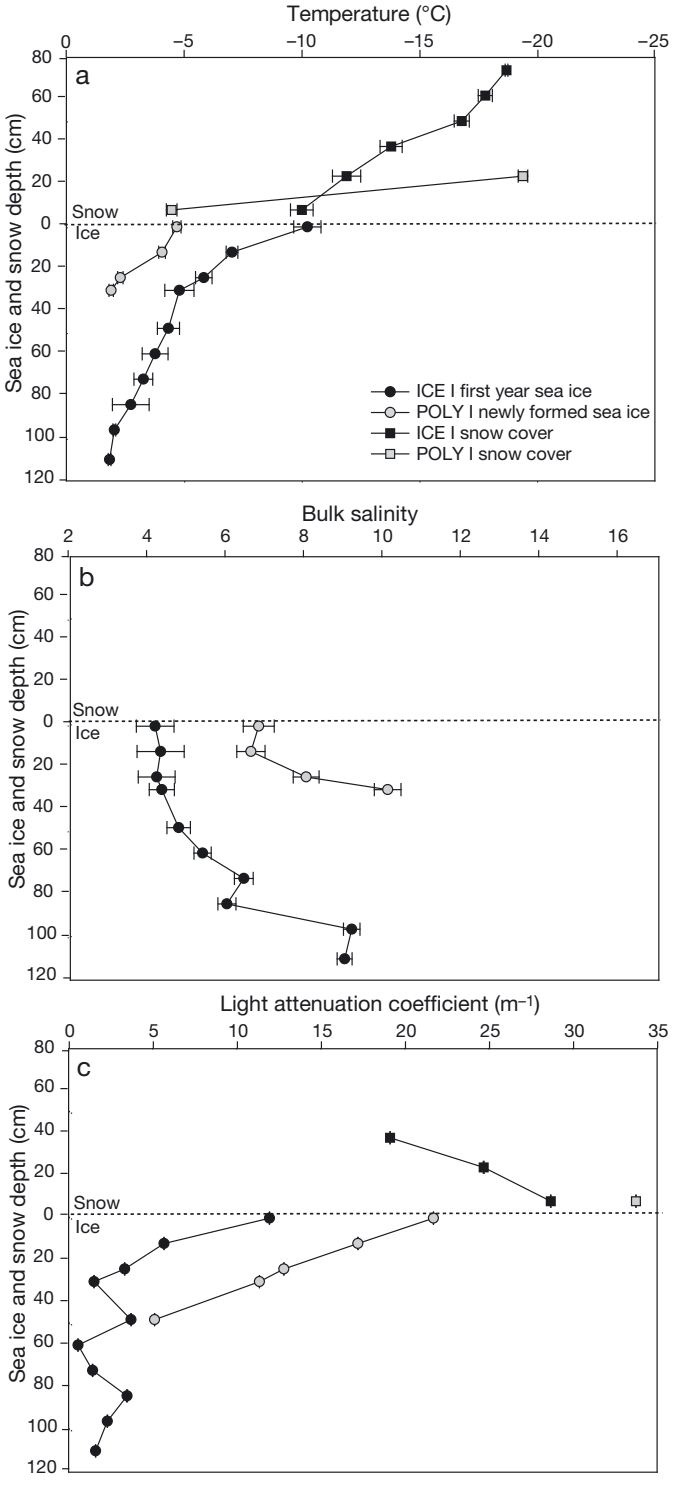

Fig. 1. Vertical profiles for ICE I and POLY I of (a) snow temperature (°C) and sea ice temperature (°C); (b) sea ice bulk salinity; and (c) snow light attenuation coefficient (m^{-1}) and sea ice light attenuation coefficient (m^{-1}). Temperatures and light attenuation coefficients above the dotted line at 0 cm are snow values. Bulk snow salinity available by refractometry (Table S1). Data points represent the average for triplicate samples; error bars indicate SD of the mean

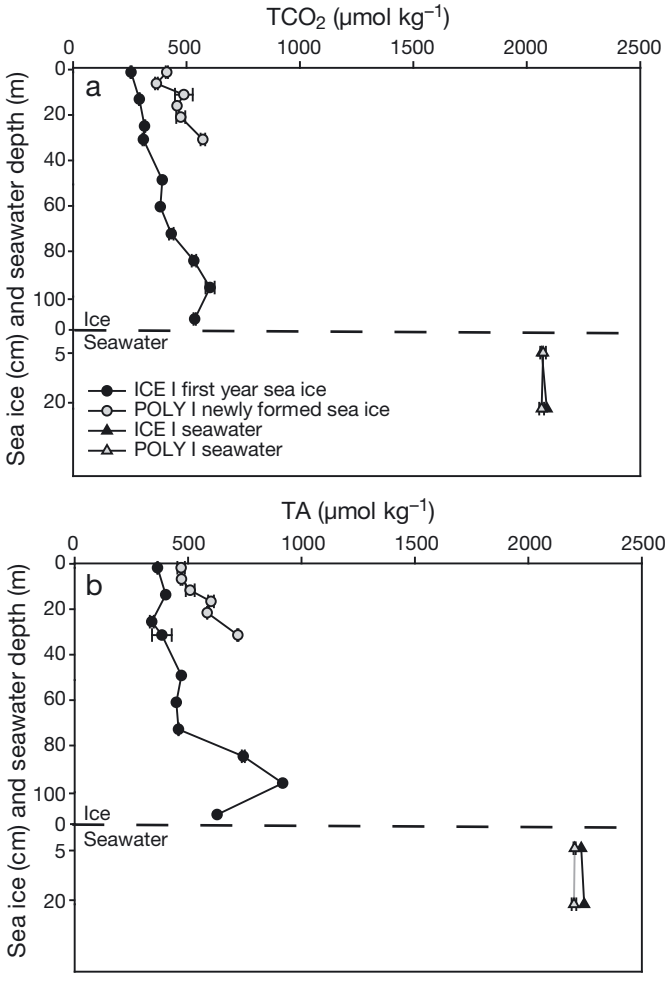

Fig. 2. Vertical concentration profiles for ICE I and POLY I of (a) TCO_2 in melted sea ice and in seawater; (b) TA in melted sea ice and in seawater. All concentrations in µmol kg^{-1}. TCO_2 and TA concentrations are from Rysgaard et al. (2013). Data points represent the average for triplicate samples; error bars indicate SD of the mean

and 520 ± 1.6 µmol kg^{-1} in the surface layers at POLY I, respectively (Fig. 2). The average TA:TCO_2 ratio in the ice was 1.26 ± 0.15 at ICE I, and 1.21 ± 0.08 at POLY I. Both values were higher than the TA:TCO_2 ratio in seawater of 1.06 ± 0.01. At ICE I, the highest TA:TCO_2 ratio (1.52 ± 0.13) was observed in the uppermost ice horizons, whereas at POLY I the highest TA:TCO_2 ratio (1.33 ± 0.10) was in the lowest horizons.

The average TCO_2 for the whole column of sea ice was 406 ± 119 µmol kg^{-1} at ICE I and 502 ± 82 µmol kg^{-1} at POLY I. These values were significantly lower than the average TCO_2 of 2070 ± 16 and 2101 ± 28 µmol kg^{-1} in the under-ice seawater at the 2 stations (Fig. 2a).

Table 1. Calcium carbonate ($CaCO_3$) concentrations in sea ice, snow, frost flowers or brine skim from different regions of the Arctic and Antarctic. SERF: Sea-ice Environmental Research Facility. $CaCO_3$ concentrations from the present study are given as mean ± SD

Area	Site	Type	Sampling year	Ice thickness (cm)	Snow depth (cm)	$CaCO_3$ concentration (µmol kg^{-1} melted sample)	Reference
Greenland	Young Sound	Thick snow cover (ICE I)	2012	110	70	430 ± 43	Present study
Greenland	Young Sound	Thin snow cover (POLY I)	2012	30	17	250 ± 27	Present study
Canada	SERF in Manitoba	Frost flowers	2013	20	1–9	2000	Rysgaard et al. (2014)
Greenland	Young Sound	Sea ice (ICE I)	2012	110	70	100–900	Rysgaard et al. (2013)
Greenland	Young Sound	Sea ice (POLY I)	2012	30	17	200–700	Rysgaard et al. (2013)
Greenland	Young Sound	Frost flowers and brine skim	2012	5–20	0	500–3000	Barber et al. (2014)
Alaska	Barrow	Frost flowers and brine skim	2009	20	0	≤25	Geilfus et al. (2013)
Greenland	Kapisigdlit	Snow cover (seasonal study)	2010	0–81	0–7	3–5	Søgaard et al. (2013)
Antarctica	Weddell Sea	Snow–ice interface	2007	15	7	1.6–6.3	Fischer et al. (2013)

The highest $CaCO_3$ concentration of 430 ± 43 µmol kg^{-1} was measured in the snow cover at ICE I, whereas a $CaCO_3$ concentration of 250 ± 27 µmol kg^{-1} was measured in the snow cover at POLY I (Table 1). Comparative values for $CaCO_3$ concentration in the underlying sea ice and from other locations are also provided (Table 1).

At the ICE I site, the highest bulk concentrations for PO_4^{3-}, $Si(OH)_4$ and NO_x, were encountered in the top 30 cm of the sea ice (Fig. 3), where they averaged 0.65 ± 0.30 µmol kg^{-1} for PO_4^{3-}, 1.29 ± 0.50 µmol kg^{-1} for $Si(OH)_4$, and 0.23 ± 0.21 µmol kg^{-1} for NO_x. These concentrations decreased with ice depth, reaching a minimum of 0.33 ± 0.06 µmol kg^{-1} for PO_4^{3-}, 0.37 ± 0.06 µmol kg^{-1} for $Si(OH)_4$ and 0.02 ± 0.009 µmol kg^{-1} for NO_x (ICE I; Fig. 3). No clear vertical distribution was observed for bulk PO_4^{3-} or NO_x concentrations in the newly formed sea ice at POLY I (Fig. 3a,b). The highest bulk $Si(OH)_4$ concentration, averaging 8.8 ± 0.70 µmol kg^{-1}, was encountered in the top 10 cm of this sea ice and decreased with ice depth, reaching an average minimum concentration of 0.9 ± 0.14 µmol kg^{-1} (POLY I; Fig. 3c). At the POLY I site, the core-average bulk concentrations were 0.50 ± 0.23 µmol kg^{-1} for PO_4^{3-}, 3.00 ± 2.5 µmol kg^{-1} for $Si(OH)_4$ and 0.83 ± 0.35 µmol kg^{-1} for NO_x (Fig. 3).

The maximum DOC concentration of 320 ± 89 µmol kg^{-1} at ICE I was encountered in interior sea ice, whereas the maximum of 430 ± 48 µmol kg^{-1} at POLY I was encountered in bottom ice layers (Fig. 4a). The lowest DOC concentration of 130 ± 45 µmol kg^{-1} was measured in the lowermost 25 cm of the sea ice at ICE I (Fig. 4a). At both ICE I and POLY I, variability was relatively high throughout the ice column (Fig. 4a).

DON concentration in the ice decreased from surface to bottom of the ice at ICE I, whereas the similar surface-ice DON concentrations at POLY I remained relatively high in the lower ice layers (Fig. 4b). The average DOC:DON ratio at ICE I was 27 ± 25, compared to the average ratio at POLY I of 24 ± 6.

Based on the bulk nutrient concentrations at ICE I and POLY I, bulk salinity, and the expected dilution line, we calculated if nutrients were depleted or if production or net accumulation of nutrients had occurred at these sites (Clarke & Ackley 1984). To calculate the dilution line, we used the average nutrient concentration and salinity measured on 18 March 2012 in the upper water column (i.e. 0–10 m, average salinity of 33; PO_4^{3-} = 0.60 ± 0.08 µmol kg^{-1} seawater, $Si(OH)_4$ = 5.20 ± 1.7 µmol kg^{-1} seawater, and NO_x = 1.40 ± 0.61 µmol kg^{-1} seawater). Values below the line indicate nutrient depletion; values above it indicate either production or net accumulation. Plots of concentrations of PO_4^{3-}, $Si(OH)_4$, NO_x, DOC and DON versus salinity in sea ice at ICE I were generally all above the dilution line, implying accumulation of nutrients; however, depletion of $Si(OH)_4$ was observed in the top sea ice sections at ICE I (see Fig. S2 in the Supplement). For the newly formed sea ice at POLY I, plots of concentrations of PO_4^{3-}, $Si(OH)_4$, NO_x, DOC and DON versus salinity were generally all above the dilution line, again implying accumulation of nutrients (see Fig. S3 in the Supplement).

3.3. Biotic parameters

Values in this section are also reported as mean ± SD for melted sea ice samples. At ICE I, volume-specific gross primary production varied vertically, from a minimum value of 0.05 ± 0.03 µg C kg^{-1} d^{-1} in the top ice layer to maximum value of 0.33 ± 0.11 µg C kg^{-1} d^{-1} in the bottom layer (Fig. 5a). For sea ice at

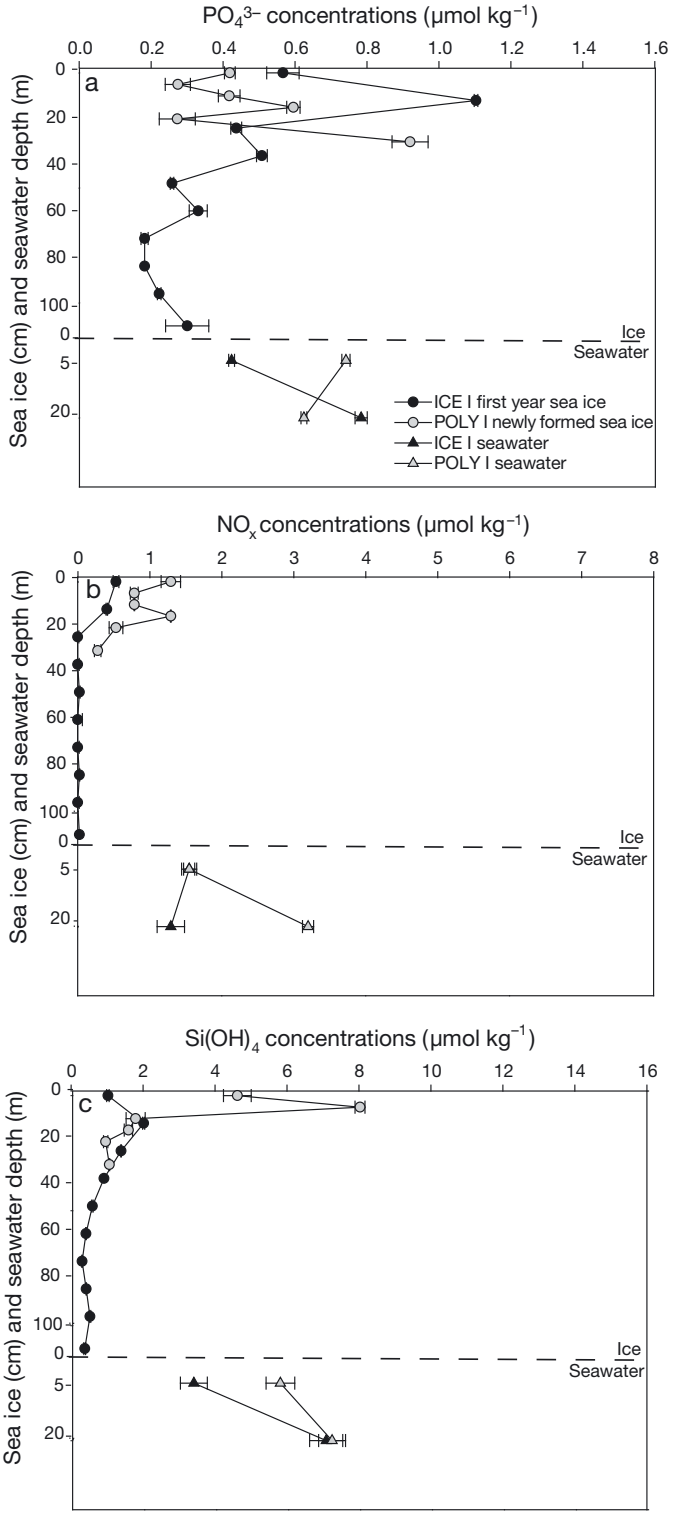

Fig. 3. Vertical profiles for ICE I and POLY I of (a) PO_4^{3-} concentrations in melted sea ice at and seawater; (b) NO_x concentrations in melted sea ice and in seawater; and (c) $Si(OH)_4$ concentrations in melted sea ice and in seawater. All concentrations in µmol kg^{-1}. Values below the dashed line at 0 cm are seawater values. Data points represent the average for triplicate samples; error bars indicate SD of the mean

POLY I this parameter showed a similar pattern, though the minimum of 0.08 ± 0.01 µg C kg^{-1} d^{-1} was slightly higher, and the maximum of 0.27 ± 0.02 µg C kg^{-1} d^{-1} was slightly lower, than at ICE I (Fig. 5a).

Bacterial carbon demand also varied vertically in the sea ice at both locations, but did not follow the distributional patterns of the primary production measurements. The maximum bacterial carbon demand was encountered in the top section of the ice: 3.44 ± 0.78 µg C kg^{-1} d^{-1} at ICE I, and 5.20 ± 0.70 µg C kg^{-1} d^{-1} at POLY I (Fig. 5b).

Depth-integrated gross primary production in the sea ice at ICE I was 0.14 ± 0.01 mg C m^{-2} d^{-1}, which was higher than the value of 0.06 ± 0.01 mg C m^{-2} d^{-1} at POLY I. The integrated bacterial carbon demand was also higher at ICE I (2.00 ± 0.31 mg C m^{-2} d^{-1}; Fig. 5b) than at POLY I (0.93 ± 0.16 mg C m^{-2} d^{-1}; Fig. 5b). The sea ice columns at both stations were thus net heterotrophic, with a carbon consumption rate of 1.86 ± 0.15 mg C m^{-2} d^{-1} at ICE I and 0.87 ± 0.15 mg C m^{-2} d^{-1} at POLY I.

Sea ice profiles of the algal biomass, expressed as chl *a*, showed the highest bulk concentrations in the bottom ice layers: 0.10 ± 0.005 at ICE I and 0.98 ± 0.05 µg chl *a* kg^{-1} at POLY I (Fig. 5c). The average algal biomass in the underlying water column was 0.01 ± 0.0005 at POLY I and 0.04 ± 0.01 µg chl *a* kg^{-1} seawater at ICE I (Fig. 5c). Based on the chl *a* concentrations and production estimates, we calculated algal biomass-specific production of 4.00 µg C µg chl *a*$^{-1}$ d^{-1} for the sea ice at ICE I and 1.00 µg C µg chl *a*$^{-1}$ d^{-1} for the ice at POLY I.

Bulk bacterial abundance varied vertically in the sea ice, from a maximum of 1.6×10^8 cells kg^{-1} in interior ice to a minimum of 4.0×10^7 cells kg^{-1} in bottom ice at ICE I (Fig. 5d). No vertical differences were observed at POLY I (Fig. 5d). Average bacterial abundance in the ice at ICE I was 5.7×10^7 cells kg^{-1} compared to 4.8×10^7 cells kg^{-1} at POLY I (Fig. 5d). Bacterial abundance in seawater was 2.1×10^8 cells kg^{-1} at ICE I and 1.5×10^8 cells kg^{-1} at POLY I (Fig. 5d). Lowest values for bacterial abundance were measured in the top of the snowpack, 5.2×10^3 cells kg^{-1} at ICE I and 4.4×10^5 cells kg^{-1} at POLY I, but increased to ~2×10^8 cells kg^{-1} at both sites in the most saline snow layer at the snow–ice interface (Table S1), as similarly observed in snow over winter sea ice near Barrow, Alaska (Ewert et al. 2013).

Total bacterial biomass in sea ice was calculated from bacterial abundance using a conversion factor of 40 fg C cell^{-1}, as determined for naturally occurring marine bacteria at high latitude by Bjørnsen & Kuparinen (1991). This calculation yielded biomass

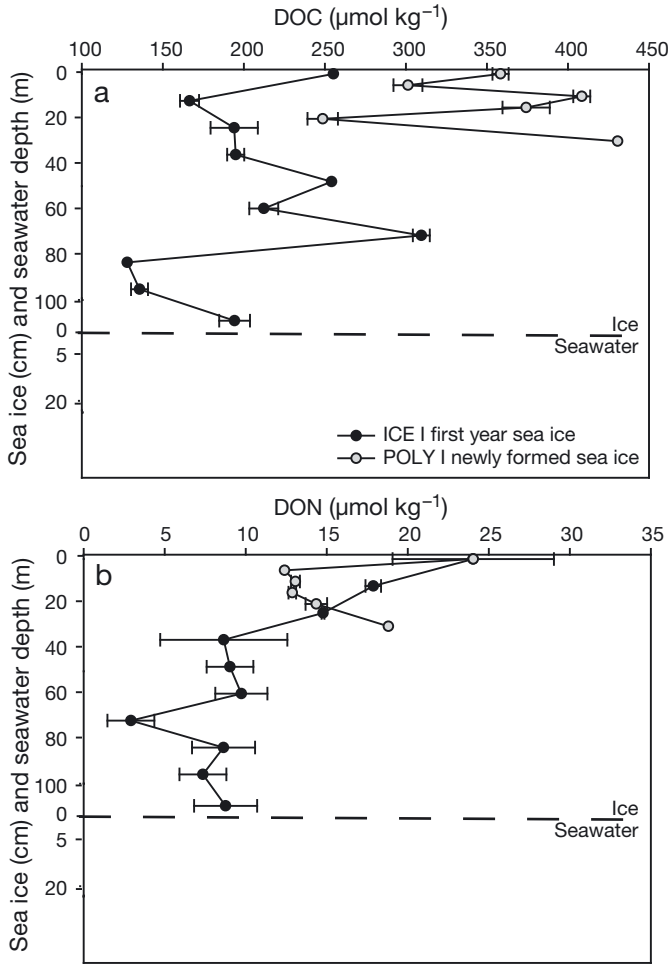

Fig. 4. Vertical profiles for ICE I and POLY I of (a) DOC concentrations in melted sea ice and in seawater; and (b) DON concentrations in melted sea ice and in seawater. All concentrations in µmol kg^{-1}. Values below the dashed line at 0 cm are sea-water values. Data points represent the average for triplicate samples; error bars indicate SD of the mean

values of 2.30 mg C m^{-2} for ICE I and 0.80 mg C m^{-2} for POLY I.

Bacterial biomass-specific production values of 0.90 mg C m^{-2} d^{-1} and 1.1 mg C m^{-2} d^{-1} were calculated for sea ice at ICE I and POLY I, respectively. Bacterial cell-specific production values of 0.03 µg C cell^{-1} d^{-1} and 0.05 µg C cell^{-1} d^{-1} were calculated for ICE I and POLY I, respectively (from data in Fig. 5b,d and calculated biomass of 2.30 mg C m^{-2} for ICE I and 0.80 mg C m^{-2} for POLY I).

Pearson correlation coefficients were calculated for sea ice primary production versus sea ice bacterial carbon demand, bacterial abundance, chl *a*, $CaCO_3$ concentration, TA, TCO_2, bulk salinity and temperature. They were also calculated for sea ice bacterial carbon demand and abundance, versus sea ice primary production, chl *a*, $CaCO_3$ concentration, TA, TCO_2, bulk salinity and temperature. For ICE I, primary production correlated positively with chl *a*, $CaCO_3$ and temperature, and negatively with bulk salinity, TCO_2 and TA, at the 95% confidence level. No other significant correlation involving primary production, bacterial carbon demand, bacterial abundance or any other factor was observed at this site. For POLY I, there was a negative correlation between primary production and both bacterial carbon demand and temperature, and between bacterial carbon demand and temperature, while a positive correlation was observed between bacterial carbon demand and both TA and $CaCO_3$ concentration (95% confidence level). No other significant correlation involving bacterial abundance and any other factor was detected for this newly formed sea ice. For both ICE I and POLY I, TA and TCO_2 correlated positively with bulk salinity, at the 95% confidence level.

4. DISCUSSION

4.1. Biological activity in first-year sea ice and newly formed sea ice

Several studies on abiotic processes and mineral formation within sea ice have highlighted the important role that sea ice plays in controlling the air–sea CO_2 flux (e.g. Grimm et al. 2016). Less attention has been paid to combined measurements of photosynthesis and respiration (or proxies for these) associated with sea ice and how biological activity may affect the carbonate system of the sea ice brine and, consequently, gas fluxes from the ice (Campbell et al. 2015, Miller et al. 2015).

The integrated pigment concentrations and photosynthetic activities in this wintertime study, reaching 0.05 to 0.06 mg chl *a* m^{-2} and 0.06 to 0.14 mg C m^{-2} d^{-1}, respectively (Fig. 5a,c), are among the lowest values reported for Greenland sea ice. Previous surveys show ranges of 0.04 to 11.5 mg chl *a* m^{-2} and 0.2 to 140 mg C m^{-2} d^{-1} (Søgaard 2014). Our low biomass values are consistent with other winter measurements in Young Sound (0.05 mg chl *a* m^{-2} in March 2005; S. Rysgaard unpubl. data) and SW Greenland (Mikkelsen et al. 2008), though our rates are lower than the only other winter rates of 0.3 to 0.8 mg C m^{-2} d^{-1} in SW Greenland (Søgaard et al. 2010). Compared to values for Arctic sea ice in general, which range from 1 to 300 mg chl *a* m^{-2} and 0.03 to 460 mg C m^{-2} d^{-1} (Arrigo 2017, van Leeuwe et al. 2018), our measurements from Young Sound are extremely low.

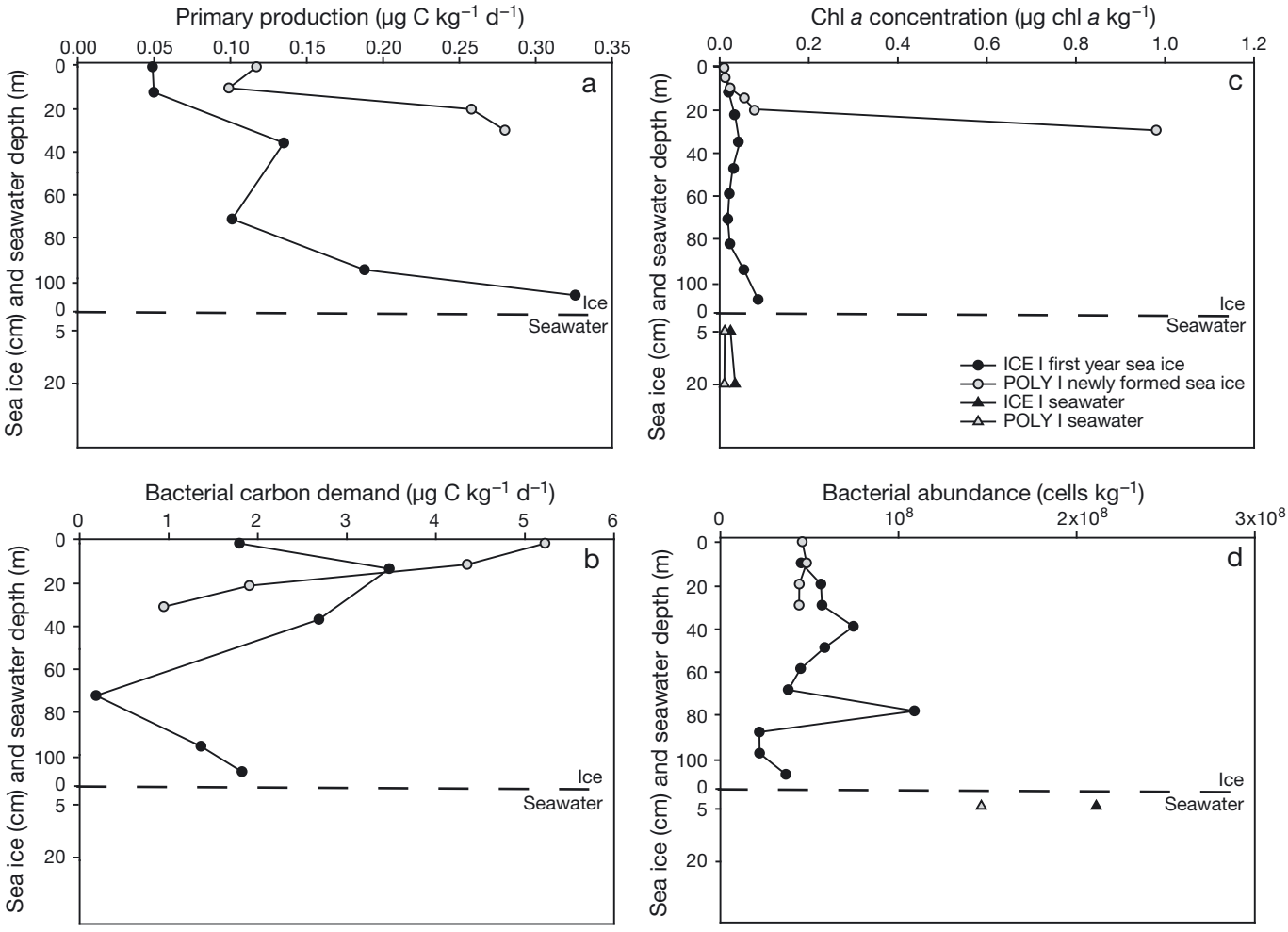

Fig. 5. Vertical profiles for ICE I and POLY I of (a) rates of primary production (µg C kg^{-1} d^{-1}) for melted sea ice; (b) bacterial carbon demand (µg C kg^{-1} d^{-1}) for melted sea ice; (c) chl *a* concentration (µg chl *a* kg^{-1}) for melted sea ice and in seawater; and (d) bacterial abundance (cells kg^{-1}) for melted sea ice and in seawater. Values below the dashed line at 0 cm are seawater values. Data points represent the average of duplicate samples

These very low algal biomass and productivity values for Young Sound can be attributed to light limitation, given the late-winter sampling date and the heavy snow cover of 70 cm at the FYI site compared to 17 cm at POLY I, as well as other features of the snow and ice. Light attenuation by snow in this study is higher than reported elsewhere (Hancke et al. 2018), particularly at the POLY I site (Fig. 1c). The fresh (and drier) snow cover at POLY I compared to the older compressed snow observed at ICE I potentially explains the higher light attenuation (Fig. 1c; see Glud et al. 2007). Previous studies have indicated that warmer sea ice shows a higher degree of backscatter and thus higher attenuation coefficient than colder sea ice due to wider brine volumes (Lund-Hansen et al. 2015). The temperature differential between sea ice at our 2 sites may help to explain the higher attenuation coefficient in the (warmer) sea ice at POLY I as compared to that at ICE I (Fig. 1a,c).

Light has previously been identified as the major limiting factor for algal productivity in sea ice, where a snow cover of 40 cm has been considered sufficient to prevent algal growth by limiting light transmission (e.g. Søgaard et al. 2010, Campbell et al. 2015, 2018). The daily average light availability at ICE I was 0.2 µmol photons m^{-2} s^{-1} (calculated from hourly *in situ* PAR and the averaged light attenuation coefficient over the depth of the ice at ICE I [Fig. 1c] and using the Lambert-Beer equation), which corresponds to less than 0.001% of the amount of light that reaches the surface of the snow. This level is considerably lower than the lowest light intensities (0.36 to 20 µmol photons m^{-2} s^{-1}) at which net photosynthesis has been previously observed in Arctic sea ice (Gra-

dinger & Ikävalko 1998, Mock & Gradinger 1999, Campbell et al. 2016). The insufficient light reaching the sea ice at ICE I in March would have prevented the development of an algal bloom, thus explaining the dominance of the heterotrophic microbial community in the ice (Fig. 5a,b). Nevertheless, the ice algae in this study were able to grow at extremely low irradiance (0.2 µmol photons m^{-2} s^{-1}). This result is comparable to a recent study in Northern Greenland, where ice algae were observed to begin to grow at a light intensity below 0.17 µmol photons m^{-2} s^{-1} (Hancke et al. 2018).

For the newly formed sea ice at POLY I, the snow cover was thinner, resulting in light availability of 2.6 µmol photons m^{-2} s^{-1} (calculated from hourly *in situ* PAR and the averaged light attenuation coefficient over the depth of the ice at POLY I [Fig. 1c] and using the Lambert-Beer equation), 10 times higher than at the ICE I site (corresponding to 0.01% of the amount of light that reached the surface of the snow). The maximum depth-integrated sea ice algal biomass of 0.06 mg chl *a* m^{-2} in the newly formed sea ice was nevertheless low (Fig. 5c) and in the same range as the maximum depth-integrated sea ice algal biomass of 0.05 mg chl *a* m^{-2} at ICE I. This similarity in algal biomass despite differences in light availability may be due to different colonization dates. The newly formed thin sea ice had been colonized within a week, while the ICE I was more than 5 months old. With more time to establish an ice-adapted algal community, a more efficient photosynthetic response might be expected in meter-thick FYI compared to thin, newly formed ice with only recently entrained algal cells. This explanation is supported by the comparative biomass-specific production rates, where the rate calculated for ICE I was 4 times the rate for the newly formed sea ice.

In addition to light limitation, we considered nutrient limitation between the FYI and newly formed sea ice. Given that bulk nutrient concentrations in the FYI were low compared to the new ice (Fig. 3) and that nutrient–salt plots indicated depletion of $Si(OH)_4$ in the FYI (Fig. 3c, Fig. S2), algae in the FYI were nutrient-limited at the time of sampling. Assuming that nutrient uptake followed the standard Redfield-Brzezinski ratio of 106C:16N:15Si:1P, then both NO_x (N:P ratio > 1) and $Si(OH)_4$ (Si:P ratio < 2) appeared to have limited algal production in the thick FYI.

In the newly formed sea ice, the higher $Si(OH)_4$ and PO_4^{3-} concentrations (Fig. 3a,c) represented a pre-bloom situation, comparing well to values reported for sea ice in other Arctic locations (Campbell et al. 2016, 2018). The NO_x concentration, however, was considerably lower than values reported elsewhere (Campbell et al. 2016, 2018; Fig. 3b). Again assuming that Redfield-Brzezinski ratios pertain to this system, then NO_x (N:P ratio > 1) but not silicate was limiting algal production in the newly formed sea ice. DNA-based analyses of this new sea ice showed that members of the genus *Nitrospina,* known for production of nitrate through nitrification, dominated the bacterial community (Barber et al. 2014), suggesting that nitrate may potentially become available within the ice to support ice algal productivity as the season progresses. This scenario is supported by measurements of nitrification in Greenland sea ice (Firth et al. 2016) and by the nutrient–salt plots for NO_x indicating NO_x accumulation in the ice (Fig. S3).

In contrast to the algal data, bacterial abundance in the sea ice was comparable between ICE I and POLY I (Fig. 5b) and both the integrated rates of cell-specific production (ICE I: 0.03 µg C $cell^{-1}$ d^{-1}; POLY I: 0.05 µg C $cell^{-1}$ d^{-1}) and biomass-specific production (ICE I: 0.90 mg C m^{-2} d^{-1}; POLY I: 1.1 mg C m^{-2} d^{-1}) were very similar in the FYI and the newly formed sea ice (see Fig. 5b,d). This similarity suggests that the heterotrophic bacterial community in the newly formed sea ice was able to establish an ice-adapted and active biomass within a week.

Our calculations of bacterial carbon demand may be under- or over-estimates because of the uncertainty inherent to bacterial growth efficiency (BGE) (we used 0.5, as for polar oceans according to Rivkin & Legendre 2001). Selection of a lower or higher BGE (0.10, 0.25, 0.90) as in other studies (Nguyen & Maranger 2011, Middelboe et al. 2012) yields values for bacterial carbon demand that range from 0.5 to 10 mg C m^{-2} d^{-1}, depending on the BGE used. Even the lowest of these values, however, is nearly 4 times higher than the highest rate measured for primary production (range of 0.06–0.14 mg C m^{-2} d^{-1}). Thus, the choice of BGE does not affect the overall conclusion that microbial activity in both types of sea ice formations examined in this study was net heterotrophic.

The accumulation of DOC and the very high DOC:DON ratios, ranging from 25 to 27, observed in sea ice at both locations (Fig. 4, Figs. S2 & S3), indicates a low-quality (nitrogen-limited) substrate for heterotrophic bacteria (Pomeroy & Wiebe 2001), suggesting that the heterotrophic community in this sea ice could be restricted in its activity even though the system is net-heterotrophic. As no correlation was observed between rates of primary production and bacterial carbon demand and the rates of primary production were very low, alternative carbon or

nitrogen sources may be contributing to the observed bacterial activity (Stewart & Fritsen 2004). One alternative source of new carbon, as well as nitrate oxidized from ammonia, may be chemoautotrophic bacterial nitrification. Nitrification has been measured in Greenland sea ice (Firth et al. 2016), and nitrifying taxa known to be chemoautotrophic were present in sea ice at both sites in this study and were dominant in the sea ice community at POLY I (Barber et al. 2014). The high DOC:DON ratios may also reflect a microbial cryoprotective response in the form of production of extracellular polysaccharide substances (Collins et al. 2008, Krembs et al. 2011). Evidence for such production at POLY I was reported previously (Barber et al. 2014). Regardless, sufficiently high bacterial production was measured at the time of sampling to conclude that the sea ice was net-heterotrophic, given the high ratios (average of 14) of bacterial production to primary production (Fig. 5b) and a bacterial carbon demand of 0.93 to 2.00 mg C m^{-2} d^{-1} (compared to 0.06–0.14 mg C m^{-2} d^{-1} for primary production). This carbon demand compares well to similarly measured rates of 0.80 to 1.80 mg C m^{-2} d^{-1} (Søgaard et al. 2010, 2013) in winter sea ice in SW Greenland and 3.80 mg C m^{-2} d^{-1} in melting sea ice of Fram Strait (Glud et al. 2014), though it is considerably lower than the rate of 26 mg C m^{-2} d^{-1} inferred by eddy correlation in winter sea ice in SW Greenland (Long et al. 2012).

Net heterotrophy is also consistent with the pre-bloom situation indicated by the low chl *a* concentrations and low rates of primary production during the study period, such that bacterial production estimates were always higher than primary production. The nutrient–salt plots also indicate that some accumulation of algal nutrients occurred in the sea ice at both locations (Figs. S2 & S3), which supports not only the very low primary productivity measured in the ice (allowing nutrients to accumulate) but also the conclusion that heterotrophic bacteria, as the most active components of the biological community, are the main source of biogenic CO_2 in winter sea ice.

4.2. Carbon dynamics in thick snow-covered winter sea ice and newly formed thin polynya sea ice

Combining the data presented in this study allowed us to consider the relative importance of biological activity and precipitation of $CaCO_3$ on the air–sea exchange of CO_2. At both locations, large deficits in bulk TCO_2 concentration were observed: −1568 ± 82 and −1701 ± 119 µmol kg^{-1} melted sea ice for POLY I and ICE I, respectively (see Fig. 2a). Assuming that the average conditions in seawater represent the conditions at ice formation (Figs. 1 & 3), the estimated sea ice-associated TCO_2 depletion was mainly controlled by brine drainage and $CaCO_3$ precipitation or dissolution, which accounted for 67 and 81% of the sea ice-associated TCO_2 deficits. We found a strong positive correlation between TA and TCO_2 versus bulk salinity, which also indicates the release of TA and TCO_2 together with brine to the underlying water column. This analysis emphasizes that the biological activity measured in the ice at both locations had a minor effect on the CO_2 system in the sea ice for the season and conditions examined.

Bacterial activity, considered the primary source of biogenic CO_2 in this sea ice, appeared to exert little influence on the precipitation and/or dissolution of $CaCO_3$, as no significant relationship was detected between $CaCO_3$ concentration and bacterial carbon demand at either ice location. A positive correlation was observed, however, between $CaCO_3$ concentration and rate of primary production in the FYI, indicating a possible coupling between $CaCO_3$ precipitation or dissolution and primary production even with the low rates measured.

The snow we sampled contained relatively high amounts of $CaCO_3$, ranging from 250 µmol kg^{-1} at POLY I to 430 µmol kg^{-1} at ICE I (Table 1). Although within the range measured in sea ice and in surface features (frost flowers and brine skim) of the ice at these 2 stations, these $CaCO_3$ concentrations are considerably higher than those reported for snow cover from other regions (Table 1).

A potential explanation for the high $CaCO_3$ values in the snow is incorporation of frost flowers into the snowpack (Rysgaard et al. 2014). In a study of frost flowers during the same campaign, very high ikaite concentrations were observed in the high-salinity (and bacteria-rich) brine skim and frost flowers within an hour of frost-flower formation on thin ice (Barber et al. 2014), and in the present study, high salinities (and bacterial abundance) were measured in the snow, particularly near the snow–ice interface, at both studied sites (Table S1). Incorporation of $CaCO_3$ crystals from frost flowers into the snow cover, together with the CO_2 that is released during $CaCO_3$ crystal precipitation, may result in snow-driven CO_2 outgassing under high wind speeds above winter sea ice, as observed during the same ice campaign by Sievers et al. (2015). Other studies have interpreted such observations as an outgassing of CO_2 from winter sea ice (Else et al. 2011, Miller et al. 2011). However, we hypothesize that CO_2 out-

gassing from winter sea ice may be attributable to loss of stored CO_2 in the snowpack. This explanation would result in a closed CO_2 loop, with wind-induced CO_2 release above the ice in winter and CO_2 uptake during spring due to undersaturation in CO_2 after $CaCO_3$ dissolution (Rysgaard et al. 2014, Søgaard 2014).

5. CONCLUSION

The biomass-specific primary production rates estimated for the newly formed sea ice and the FYI that we examined indicated that a more efficient photosynthetic response was observed in the FYI ice with its established microbial community compared to the algal cells newly entrained into the young ice. In contrast, bacterial cell-specific production rates were similar at both of these sea ice sites. This pattern suggests that the heterotrophic communities in the newly formed sea ice were able to establish an ice-adapted and active bacterial biomass within a week, whereas the algal community needed more time to establish. Net heterotrophy characterized both ice types.

Although both biotic and abiotic processes can influence the inorganic carbon dynamics within the sea ice, the influence of primary and bacterial productivity on the measured deficit in TCO_2 concentration in this winter sea ice, relative to surface water concentrations, was minor. The TCO_2 depletion was controlled mainly by the abiotic processes of brine drainage and $CaCO_3$ precipitation or dissolution, accounting for 67 and 81% of the sea ice-associated TCO_2 deficit at the 2 sites. The role of biology in modulating inorganic carbon dynamics in the sea ice of Young Sound is apparently delayed until the spring and summer seasons. This study has also shown that $CaCO_3$ crystal concentrations in the snow cover at both stations were high, which could have major implications for understanding the source of wind-induced CO_2 degassing over winter sea ice.

Acknowledgements. We thank Martin E. Blicher and Michael S. Schrøder for statistical assistance, Egon Frandsen, Kunuk Lennert and Ivali Lennert for outstanding assistance in the field, and Shelly Carpenter for laboratory support. We greatly appreciate the meteorological data provided by Asiaq (Greenland Survey). This study received financial support from the Canada Excellence Research Chair (CERC) program, the Danish Agency of Science, Technology and Innovation, the Arctic Research Centre of Aarhus University, the Commission for Scientific Research in Greenland, and the US National Science Foundation (OPP–ARC–1203267 to J.W.D.). D.H.S. was supported financially by the Commission for Scientific Research in Greenland (KVUG). L.M. was funded by a postdoctoral grant from the Greenland Research Council. This is a contribution to the Arctic Science Partnership (ASP), www.asp-net.org.

LITERATURE CITED

Arrigo KR (2017) Sea ice as a habitat for primary producers. In: Thomas DN (ed) Sea ice, 3nd edn. Wiley-Blackwell Publishing, Oxford, p 352–369

Barber DG, Ehn JK, Pućko M, Rysgaard S and others (2014) Frost flowers on young Arctic sea ice: the climatic, chemical and microbial significance of an emerging ice type. J Geophys Res Atmos 119:11593–11612

Bjørnsen PK, Kuparinen J (1991) Determination of bacterioplankton biomass, net production and growth efficiency in the Southern Ocean. Mar Ecol Prog Ser 71:185–194

Boone W, Rysgaard S, Kirillov S, Dmitrenko I and others (2017) Circulation and fjord-shelf exchange during the ice-covered period in Young Sound-Tyrolerfjord, Northeast Greenland (74°N). Estuar Coast Shelf Sci 194: 205–216

Campbell K, Mundy CJ, Barber DG, Gosselin M (2015) Characterizing the sea ice algae chl *a*–snow depth relationship over Arctic spring melt using transmitted irradiance. J Mar Syst 147:76–84

Campbell K, Mundy CJ, Landy JC, Delaforge A, Michel C, Rysgaard S (2016) Community dynamics of bottom-ice algae in Dease Strait of the Canadian Arctic. Progr Oceanogr 149:27–39

Campbell K, Mundy CJ, Belzile C, Delaforge A, Rysgaard S (2018) Seasonal dynamics of algal and bacterial communities in Arctic sea ice under variable snow cover. Polar Biol 41:41–58

Clarke DB, Ackley SF (1984) Sea ice structure and biological activity in the Antarctic marginal ice zone. J Geophys Res 89:2087–2095

Collins RE, Carpenter SD, Deming JW (2008) Spatial heterogeneity and temporal dynamics of particles, bacteria, and pEPS in Arctic winter sea ice. J Mar Syst 74:902–917

Collins RE, Rocap G, Deming JW (2010) Persistence of bacterial and archaeal communities in sea ice through an Arctic winter. Environ Microbiol 12:1828–1841

Deming JW (2010) Sea ice bacteria and viruses. In: Thomas DN, Dieckmann GS (eds) Sea ice, 2nd edn. Wiley-Blackwell Publishing, Oxford, p 248–282

Dmitrenko IA, Kirillov SA, Rysgaard S, Barber D and others (2015) Polynya impacts on water properties in a Northeast Greenland fjord. Estuar Coast Shelf Sci 153:10–17

Else BGT, Papakyriakou TN, Galley RJ, Drennan WM, Miller LA, Thomas H (2011) Wintertime CO_2 fluxes in an Arctic polynya using eddy covariance: evidence of enhanced air–sea gas transfer during ice formation. J Geophys Res C Oceans 116:C00G03

Eronen-Rasimus E, Kaartokallio H, Lyra C, Autio R, Kuosa H, Dieckmann GS, Thomas DN (2014) Bacterial community dynamics and activity in relation to dissolved organic matter availability during sea-ice formation in a mesocosm experiment. MicrobiologyOpen 3:139–156

Ewert M, Carpenter SD, Colangelo-Lillis J, Deming JW (2013) Bacterial and extracellular polysaccharide content of brine-wetted snow over Arctic winter first-year sea ice. J Geophys Res C Oceans 118:726–735

Fernández-Méndez M, Katlein C, Rabe B, Nicolaus M and others (2015) Photosynthetic production in the central Arctic Ocean during the record sea-ice minimum in 2012. Biogeosciences 12:3525–3549

Firth E, Carpenter SD, Sørensen HL, Collins RE, Deming JW (2016) Bacterial use of choline to tolerate salinity shifts in sea ice brines. Elem Sci Anth 4:000120

Fischer M, Thomas DN, Krell A, Nehrke G and others (2013) Quantification of ikaite in Antarctic sea ice. Antarct Sci 25:421–432

Geilfus NX, Carnat G, Dieckmann GS, Halden N and others (2013) First estimates of the contribution of $CaCO_3$ precipitation to the release of CO_2 to the atmosphere during young sea ice growth. J Geophys Res 118:244–255

Geilfus NX, Galley RJ, Else BGT, Campbell K and others (2016) Estimates of ikaite export from sea ice to the underlying seawater in a sea ice-seawater mesocosm. Cryosphere 10:2173–2189

Glud RN, Rysgaard S, Kühl M, Hansen JW (2007) The sea ice in Young Sound: implications for C cycling. In: Rysgaard S, Glud RN (eds) Carbon cycling in Arctic marine ecosystems: case study Young Sound. Bioscience, Vol 58. Commission for Scientific Research in Greenland (Meddelser om Grønland), Copenhagen, p 62–85

Glud RN, Rysgaard S, Turner G, McGinnis DF, Leakey RJG (2014) Biological and physical-induced oxygen dynamics in melting sea ice of the Fram Strait. Limnol Oceanogr 59:1097–1111

Gradinger R (2009) Sea-ice algae: major contributors to primary production and algal biomass in the Chukchi and Beaufort Seas during May/June 2002. Deep Sea Res II 56:1201–1212

Gradinger R, Ikävalko J (1998) Organism incorporation into newly forming Arctic sea ice in the Greenland Sea. J Plankton Res 20:871–886

Grasshoff K, Erhardt M, Kremling K (1983) Methods of seawater analysis, 2nd edn. Verlag Chemie, Weinheim

Grimm R, Notz D, Glud RN, Rysgaard S, Six KD (2016) Assessment of the sea-ice carbon pump: insights from a three-dimensional ocean-sea-ice-biogeochemical model (MPIOM/HAMOCC). Elem Sci Anth 4:000136

Hancke K, Lund-Hansen LC, Lamare ML, Pedersen SH, King MD, Andersen P, Sorrell BK (2018) Extreme low light requirement for algae growth underneath sea ice: a case study from Station Nord, NE Greenland. J Geophys Res C Oceans 123:1–16

Jensen LM, Rasch M, Schmidt NM (eds) (2013) Zackenberg ecological research operations, 18th annual report, 2012. Aarhus University, Danish Centre for Environment and Energy, Aarhus

Johnson KM, Wills KD, Butler DB, Johnson WK, Wong CS (1993) Coulometric total carbon dioxide analysis for marine studies: maximizing the performance of an automated gas extraction system and coulometric detector. Mar Chem 44:167–187

Kern S, Khvorostovsky K, Skourup H, Rinne E and others (2015) The impact of snow depth, snow density and ice density on sea ice thickness retrieval from satellite radar altimetry: results from ESA-CCI Sea Ice ECV Project Round Robin Exercise. Cryosphere 9:37–52

Krembs C, Eicken H, Deming JW (2011) Exopolymer alteration of physical properties of sea ice and implications for ice habitability and biogeochemistry in a warmer Arctic. Proc Natl Acad Sci USA 108:3653–3658

Long MH, Koopmans D, Berg P, Rysgaard S, Glud RN, Søgaard DH (2012) Oxygen exchange and ice melt measured at the ice-water interface by eddy correlation. Biogeosciences Discuss 8:11255–11284

Lund-Hansen LC, Markager S, Hancke K, Stratmann T, Rysgaard S, Ramløv H, Sorrell BK (2015) Effects of sea-ice light attenuation and CDOM absorption in the water below the Eurasian sector of central Arctic Ocean (>88°N). Polar Res 34:23978

Marion GM (2001) Carbonate mineral solubility at low temperatures in the Na-K-Mg-Ca-H-Cl-SO_4-OH-HCO_3-CO_3-CO_2-H_2O system. Geochim Cosmochim Acta 65: 1883–1896

Middelboe M, Glud RN, Sejr MK (2012) Bacterial carbon cycling in a subarctic fjord: a seasonal study on microbial activity, growth efficiency, and virus-induced mortality in Kobbefjord, Greenland. Limnol Oceanogr 57: 1732–1742

Mikkelsen DM, Rysgaard S, Glud RN (2008) Microalgal composition and primary production in Arctic sea ice: a seasonal study from Kobbefjord (Kangerluarsunnguaq), West Greenland. Mar Ecol Prog Ser 368:65–74

Miller LA, Papakyriakou TN, Collins RE, Deming JW and others (2011) Carbon dynamics in sea ice: a winter flux time series. J Geophys Res C Oceans 116:C02028

Miller LA, Fripiat F, Else BGT, Bowman JS and others (2015) Methods for biogeochemical studies of sea ice: the state of the art, caveats and recommendations. Elem Sci Anth 3:000038

Mock T, Gradinger R (1999) Determination of Arctic ice algal production with a new *in situ* incubation technique. Mar Ecol Prog Ser 177:15–26

Nguyen D, Maranger R (2011) Respiration and bacterial carbon dynamics in Arctic sea ice. Polar Biol 34: 1843–1855

Nomura D, Eicken H, Gradinger R, Shirasawa K (2010b) Rapid physically driven inversion of the air–sea ice CO_2 flux in the seasonal landfast ice off Barrow, Alaska after onset of surface melt. Cont Shelf Res 30:1998–2004

Papadimitriou S, Kennedy H, Norman L, Kennedy DP, Dieckmann GS, Thomas DN (2012) The effect of biological activity, $CaCO_3$ mineral dynamics, and CO_2 degassing in the inorganic carbon cycle in sea ice in late winter–early spring in the Weddell Sea, Antarctica. J Geophys Res C Oceans 117:C08011

Pedersen JBT, Kaufmann LH, Kroon A, Jakobsen BH (2010) The northeast Greenland Sirius Water Polynya dynamics and variability inferred from satellite imagery. Geogr Tidsskr 110:131–142

Petrich C, Eicken H (2010) Growth structure and properties of sea ice. In: Thomas DN, Dieckmann GS (eds) Sea ice, 2nd edn. Wiley-Blackwell Publishing, Oxford, p 425–469

Platt T, Gallegos CL, Harrison WG (1980) Photoinhibition of photosynthesis in natural assemblages of marine phytoplankton. J Mar Res 38:687–701

Pomeroy LR, Wiebe WJ (2001) Temperature and substrate as interactive limiting factors for marine heterotrophic bacteria. Aquat Microb Ecol 23:187–204

Rivkin RB, Legendre L (2001) Biogenic carbon cycling in the upper ocean: effects of microbial respiration. Science 291:2398–2400

Rysgaard S, Glud RN, Sejr MK, Bendtsen J, Christensen PB (2007) Inorganic carbon transport during sea-ice growth and decay: a carbon pump in polar seas. J Geophys Res C Oceans 112:111–118

Rysgaard S, Bendtsen J, Petersen LT, Ramløv J, Glud RN

(2009) Increased CO_2 uptake due to sea ice growth and decay in the Nordic Seas. J Geophys Res C Oceans 114:C09011

Rysgaard S, Bendtsen J, Delille B, Dieckmann GS and others (2011) Sea ice contribution to the air-sea CO_2 exchange in the Arctic and Southern Oceans. Tellus B Chem Phys Meterol 63:823–830

Rysgaard S, Søgaard DH, Cooper M, Pućko M and others (2013) Ikaite crystal distribution in winter sea ice and implications for CO_2 system dynamics. Cryosphere 7: 707–718

Rysgaard S, Wang F, Galley RJ, Grimm R and others (2014) Temporal dynamics of ikaite in experimental sea ice. Cryosphere 8:1469–1478

Sievers J, Sørensen LL, Papakyriakou T, Else B, Sejr MK, Søgaard DH, Barber D, Rysgaard S (2015) Winter observations of CO_2 exchange between sea ice and the atmosphere in a coastal fjord environment. Cryosphere 9: 1701–1713

Smith REH, Clement P (1990) Heterotrophic activity and bacterial productivity in assemblages of microbes from sea ice in the high Arctic. Polar Biol 10:351–357

Søgaard DH (2014) Biological activity and calcium carbonate dynamics in Greenland sea ice—implication for the inorganic carbon cycle. PhD dissertation, Greenland Climate Research Centre, Greenland Institute of Natural Resources, Nuuk

Søgaard DH, Kristensen M, Rysgaard S, Glud RN, Hansen PJ, Hilligsøe KM (2010) Autotrophic and heterotrophic activity in Arctic first-year sea ice: seasonal study from Malene Bight, SW Greenland. Mar Ecol Prog Ser 419: 31–45

Søgaard DH, Thomas DN, Rysgaard S, Glud RN and others (2013) The relative contribution of biological and abiotic processes to carbon dynamics in subarctic sea ice. Polar Biol 36:1761–1777

Sørensen M (2012) Walrus Island—a pivotal place for high Arctic palaeo-Eskimo societies in Northeast Greenland. Etud Inuit 36:183–205

Steemann Nielsen E (1952) The use of radio-active carbon (C^{14}) for measuring organic production in the sea. ICES J Mar Sci 18:117–140

Stewart FJ, Fritsen CH (2004) Bacteria–algae relationships in Antarctic sea ice. Antarct Sci 16:143–156

van Leeuwe MA, Tedesco L, Arrigo KR, Assmy P and others (2018) Microalgal community structure and primary production in Arctic and Antarctic sea ice: a synthesis. Elem Sci Anth 6:4

Weeks WF, Ackley SF (1986) The growth, structure, and properties of sea ice. In: Untersteiner N (ed) The geophysics of sea ice. NATO ASI B146. Plenum Press, New York, NY

Editorial responsibility: Peter Steinberg, Sydney, New South Wales, Australia

Submitted: April 17, 2018; Accepted: January 13, 2019
Proofs received from author(s): February 4, 2019